ADVANCED MATERIALS INTERFACES
Open Access
www.advmatinterfaces.de

Cellulosic Nanofibers Utilizing a Silicone Elastomeric Core to Form Stretchable Paper

*Joab S. Dorsainvil, Matthew S. Brown, Zahra Rafiee, Anwar Elhadad, Seokheun Choi, and Ahyeon Koh**

Paper, an inexpensive material with natural biocompatibility, non-toxicity, and biodegradability, allows for affordable and cost-effective substrates for unconventional advanced electronics, often called papertronics. On the other hand, polymeric elastomers have shown to be an excellent success for substrates of soft bioelectronics, providing stretchability in skin wearable technology for continuous sensing applications. Although both materials hold their unique advantageous characteristics, merging both material properties into a single electronic substrate reimagines paper-based bioelectronics for wearable and patchable applications in biosensing, energy generation and storage, soft actuators, and more. Here, a breathable, light-weighted, biocompatible engineered stretchable paper is reported via coaxial nonwoven microfibers for unconventional bioelectronic substrates. The stretchable papers allow intimate bioconformability without adhesive through coaxial electrospinning of a cellulose acetate polymer (sheath) and a silicone elastomer (core). The fabricated cellulose-silicone fibers exhibit a greater percent strain than commercially available paper while retaining hydrophilicity, biocompatibility, combustibility, disposable, and other natural characteristics of paper. Moreover, the nonwoven stretchable cellulose-silicone fibrous mat can adapt conventional printing and fabrication process for paper-based electronics, an essential aspect of advanced bioelectronic manufacturing.

1. Introduction

Natural materials such as paper and cellulose derivatives have become of interest for flexible electronics in the past decade. Paper depends on cellulose fibers from wood pulp found in plants that are compressed together to form thin sheets of cellulose fibers. Lignin and Hemicellulose are two polymers found within plants' secondary cell walls that significantly impact cellulose fibers' physical and chemical properties.[1–3] The 2D fibrous material has been used for over 2000 years, likely because of its unique properties, including flexibility, inexpensiveness, biocompatibility, hydrophilicity, biodegradability, environmentally favorable, and highly abundant.[4–6] With advanced bioelectronics, paper has adopted paper-functional electronics for sensing,[7–9] energy production,[10–12] and various other biomedical and pharmaceutical applications. The Whitesides group first utilized paper for an inexpensive bioassay that detects analytes like glucose and protein by patterning hydrophobic barriers to form microfluidic channels.[13–15] Additionally, paper is an ideal habitat for immobilizing microorganisms or biorecognition reagents because of its porous and hydrophilic nature. Therefore, the paper can realize the range of bioelectronic applications from sensors to batteries utilizing biological prowess of enzymes and bacteria while aided by printed electronics;[16,17] however, papers as an electronic substrate challenges versatility for wearable and biointegrated bioelectronics. Although paper is flexible, there pose issues with the mechanical mismatch between paper and the evolving, living organ (e.g., the epidermal layer of skin). For instance, the elastic modulus of the epidermal layer is ≈140 kPa and has a strain of 30% and 100% at joints, while most ridged electronic devices fail at a strain of 3%, which includes the strain to failure of paper.[13–15] The mechanical mismatch of paper to skin presents long-term wearability issues such as delamination, non-conformal contact with the skin during strenuous movement, and device deformation, ultimately leading to device failure.

J. S. Dorsainvil, M. S. Brown, A. Koh
Department of Biomedical Engineering
State University of New York at Binghamton
Binghamton, NY 13920, USA
E-mail: akoh@binghamton.edu
Z. Rafiee, A. Elhadad, S. Choi
Department of Electrical and Computer Engineering
State University of New York at Binghamton
Binghamton, NY 13920, USA

The ORCID identification number(s) for the author(s) of this article can be found under https://doi.org/10.1002/admi.202300487

DOI: 10.1002/admi.202300487

Soft bioelectronics has recently highlighted wearable technology due to its unique mechanical properties that allow for bending, twisting, folding, and stretching.[19–21] Soft elastomeric polymers that mimic the skin's mechanical properties have been used for electronic substrates to maintain conformal contact with the curvilinear surface of the skin during deformations.[19–21] Various soft bioelectronics platforms for wearable and implantable devices have demonstrated continuous monitoring and stimulation of physiological information. Examples include noninvasive 3D microfluidic biosensors that detect biomarkers in sweat or saliva,[22–26] patterned microelectronics such as LED displays on stretchable rubber,[27] an inkjet-printed transistor array on a silicone elastomer,[16] and breathable porous biosensors for free gas exchange.[17,18]

To take advantage of paper-based electronics and soft bioelectronics, a single fiber structure has been designed for building units of stretchable paper consisting of silicone elastomers and cellulose. Electrospinning fabricates a nonwoven fibrous architecture like paper. We hypothesize that coaxial electrospinning can employ a core-sheath nanofiber structure of an elastomeric core to a cellulose polymeric sheath. By altering electrospinning processing parameters,[19,20] fiber morphology,[21] core-sheath structure,[22] and other physical properties can be modified to allow for both elastomer and cellulose polymer to coexist into a single fiber creating a stretchable paper.[23] Herein, a nanofibrous substrate integrating a silicone elastomer and cellulose-based polymer to create a stretchable paper. While the substrate retains the natural properties of cellulose paper, the nonwoven 3D fibrous matrix can stretch up to 45% at max strength. This work aims to present the use of stretchable paper for existing technologies in paper-based bioelectronics by demonstrating a stackable microbial fuel cell (MFC) device to have a comparable power output. The stretchable paper aspires to bridge the gap between soft bioelectronics and paper-based bioelectronics with stretchability and paper-based attributes in a single fibrous mat.

2. Results and Discussion

2.1. Fabrication and Characterization of Coaxial Silicone-Cellulose Microfibrous Nonwoven Mat

Electrospinning realizes the stretchable papers for biointerfaced paper-based bioelectronics. The coaxial microfibrous nonwoven electrospun mat with a silicone elastomer and a cellulose polymer for core and sheath, respectively, can be laminated on the skin along with mechanical deformation (**Figure 1**A) without the assistance of adhesives. Similar to conventional paper, such as US Letter printing paper (fibers 15.01 ± 3.03 μm in diameter), the coaxial electrospun mat has a nonwoven structure of cellulose fibers (0.91 ± 0.23 μm in diameter) with an elastomeric core, creating a 2D porous sheet (Figure 1B,C). Cellulose acetate (CA), a cellulose derivative, was selected for sheath material because cellulose is poorly soluble in organic solvents and thus incapable of electrospinning.[24] Then, CA sheath were converted to cellulose II by deacetylation using ethanol, and alkaline sodium hydroxide.[25] Although conventional paper is made from cellulose I—the most natural form, cellulose I is not the most thermodynamically stable material due to its molecular structure of parallel cellulosic chains. On the other hand, cellulose II exhibits more excellent thermodynamic structural stability due to hydrogen bonds through its antiparallel cellulose chains.[26] Nevertheless, both types of cellulose hold necessary characteristics for paper-based electronics, such as wicking, hydrophilicity, and combustibility.

A coaxial electrospinning setup allowed controllable production of the fibrous mat by modifying processing parameters such as solution viscosity, solvent composition, applied voltage, tip-to-collector distance, and type of collector. Different solvent systems were explored to find the optimal polymer concentration of CA for fiber morphology (Table S1, Supporting Information). Trifluoroacetic acid (TFA), acetone/dimethylacetamide (DMA), and acetone/dimethylformamide (DMF) were used in varying weight percentages of polymer solutions. The CA solution with TFA solvent formed a smooth and dense nanofibrous mat with minimal beading when electrospun with the silicone elastomer coaxially. While TFA is an excellent solvent for dissolving cellulose derivatives,[27] issues arose with encapsulating the silicone elastomer. This could be due to the strong acid etching of the silicone elastomer before curing occurs.[28] A 2:1 ratio of acetone to DMA resembled fibers with beads and larger fiber diameters. However, again, issues arose with the encapsulation of the elastomeric core. An 85:15 ratio of acetone to DMF solvent system was explored as DMF is a widely used solvent, mainly for CA fibers.[24,5] With our sheath solution encapsulating our core solution, understanding the solvent compatibility of DMF with the core solution is integral for coaxial electrospinning. DMA and DMF are acceptable solvents for dissolving cellulose acetate because they are polar aprotic solvents[29] and have great volatility for evaporation rate before deposition on the collector plate.[24,30–31] Although they are both similar solvents in their chemical structure, DMF has a hydrogen atom demonstrating hydrogen bonding while DMA has a methyl group.[32] With DMF, hydrogen bonding interactions have been reported to be a prime motivator for cellulose dissolution.[29] In addition, DMF has negligible etching on silicone elastomers despite being a strong polar solvent.[28,33] The optimized ratio and solvent composition, 17 wt.% CA in 85:15 acetone/DMF created a fiber mat with minimal beading and showed a distinctive single fiber core-sheath structure.

For introducing elastomeric mechanics in single microfiber, polydimethylsiloxane (PDMS) and DuPont's Liveo Soft Silicone Adhesive (SSA) were electrospun for the core of coaxial fibers. Our experimental setup consisted of testing PDMS at the base to cure ratios of 30:1 and 10:1 with our three solvent systems for CA. In our previous work, PDMS fibers were formed using a 30:1 ratio with 10% added tetrahydrofuran (THF) solvent to reduce viscosity for coaxial electrospinning while templated with polyvinylpyrrolidone (PVP) as a sheath. However, coaxial electrospinning of the PDMS fibers using the CA polymer proved challenging due to poor encapsulation of the PDMS core with the addition of THF. The SSA elastomer works as a two-part system with a low mixing viscosity and transparent appearance before and after curing. The SSA elastomer has a lower modulus of elasticity of 75 to 308 kPa (Table S2, Supporting Information), while PDMS has a modulus of elasticity of ≈360 to 870 kPa.[34] Similar to our experimental setup for PDMS, we used the recommended 1:1 part A to part B ratio for our three CA solvent

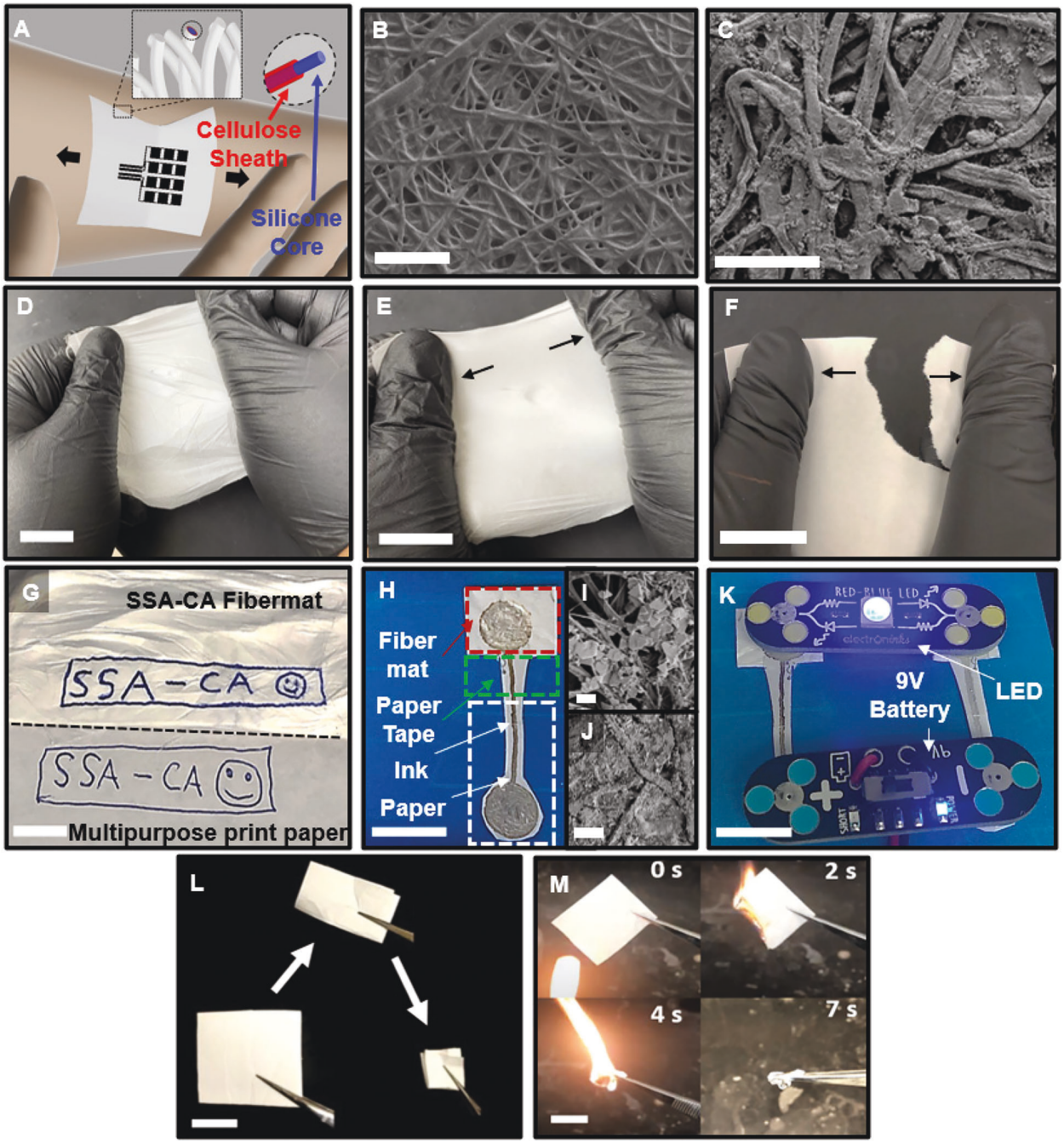

Figure 1. Characteristics of stretchable paper, SSA-CA fiber mat. A) Schematic demonstration of mechanical biocompatibility of SSA-CA fibrous mat. SEM images of B) SSA-Cellulose fiber mat (Scale bar, 20 µm) compared to C) multipurpose printer paper (scale bar, 100 µm). D) Optical images of fabricated 2D nonwoven SSA-CA fibrous mat (scale bar, 2 cm) and E) demonstrated stretchability under strain (scale bar, 2 cm), while F) US Letter paper ripped from stretching (scale bar, 2 cm). G) Ballpoint pen drawn over SSA-CA fiber mat (top) and print paper (bottom) (scale bar, 10 mm). H) SSA-CA fiber mats assembled to print paper with conductive ink (scale bar, 10 mm). SEM Images conductive ink on I) SSA-CA fiber mat (scale bar, 3 µm) and J) print paper (scale bar, 40 µm). K) Simple functional circuit demonstration of LED over fiber mat with battery over conductive ink (scale bar, 10 mm). L) Fiber mat being folded in twofolds (Scale bar, 20 mm). M) Flammability of SSA-CA fiber within 7 s (Scale bar, 20 mm).

systems. Although SSA has an initial low viscosity and does not require a solvent, we tested the elastomer in added THF in 0%, 10%, and 20% (Table S3, Supporting Information). The increase in THF concentration aided in effective taylor cone formation during electrospinning due to lowering the viscosity of the SSA, allowing minimal solvent miscibility for CA to encapsulate the SSA.

After optimization of processing parameters, we set the sheath solution at 17 wt.% CA in 85:15 acetone/DMF, and the core solution was set to a 1:1 ratio of SSA two-part system in 20% THF.

The optimal solution concentration and additive solvents refine electrospinable viscosity and enable the core to be adequately encapsulated by the interface between the core and sheath (Figure S1, Supporting Information). The electrospun SSA-CA fibrous nonwoven mat does not exhibit ripping under stretch, while US letter printing paper visibly tears along the paper's surface (Figure 1D–F).

To test its printability and writability, we used a ballpoint pen to write over the stretchable paper (Figure 1G). In Figure 1H, conductive ink was deposited to create a straightforward circuit design over the stretchable paper (red dotted box), paper tape (green dotted box), and printing paper (white dotted box). The SEM images of the contact pads on the SSA-CA fiber mat (Figure 1I) and printing paper (Figure 1J) confirm the printability of the conductive ink into the nanofibers of the SSA-CA fiber mat similar to printing paper. The conductive ink's metallic silver flakes (resistivity of 1 Ω cm^{-2}) were integrated within the 3D fibers network, which is an essential feature for reliable and robust electrical functions of the paper-based bioelectronics. Figure 1K demonstrates the electrical functions of the written contact pads on the fabricated stretchable fibrous substrates with a LED circuit and power module connected to a 9 V. With the ability to fold (Figure 1L), patterning each side with a different circuit could create more complex circuit systems. The nonwoven SSA-CA fiber mats (40 mm × 40 mm) combust within 7 s (Figure 1M), displaying their ease of disposal. As demonstrated by the experimental comparisons, the SSA-CA fiber mat certainly holds its paper-based qualities compared to compressed cellulose fibers like printing paper. Other works demonstrating the disposal of paper-based devices through combustion demonstrate burning times of fifteen seconds[35] and 30 s.[36] The fabricated SSA-CA achieves combustion in 7 s, twice as fast as Whatman filter papers. Unlike the highly flammable nitrocellulose paper, which is hazardous due to its rapidly flammable properties,[37] the SSA-CA fiber mat is not as flammable, making it safe and easy for disposal.

2.2. Physical and Chemical Characterization of Electrospun Coaxial Silicone-Cellulose Fibrous Mat

The fabricated coaxial electrospun mat morphology was analyzed for fiber diameter, sheath thickness, and core diameter. The average fiber diameter of the SSA-CA fibers was 1.38 ± 0.37 μm and 0.91 ± 0.23 μm before and after deacetylation, respectively, showing statistical insignificance (**Figure 2**A,B). By converting CA into cellulose II by deacetylation using 0.05 M NaOH and ethanol, the fibers still resemble a nonwoven fiber mat but with a coarse appearance to the sheath of the fibers (Figure 2C). The SEM and confocal images (Figure 2D,E) confirm the structural integrity of the coaxial architecture. With the core structure and sheath being coaxial, during the electrospinning process, the interface between core and sheath shows minimal mixing in Figure 2E, allowing for polymer and elastomer to form a miscible region at the interface. The miscibility at the interface becomes advantageous for the cellulose sheath as it allows for the sheath to take advantage of the elastomer's stretchability. The sheath of the fiber was determined to be 267.01 ± 84.86 nm thick, and the core fiber had a diameter of 476.48 ± 60.77 nm.

Figure 2F,G shows Fourier-transform infrared (FTIR) spectroscopy spectrums of the coaxial SSA-CA electrospun fibers compared to the SSA elastomer and the SSA-CA fiber mat before and after the deacetylation process. The FTIR spectrum of the SSA elastomer exhibit peaks at the 1019 cm^{-1} wavelengths indicating the presence of the siloxane groups. For the SSA-CA fiber mat, an additional peak at 1738 cm^{-1} presents in addition to the siloxane peak, indicating the presence of the carbonyl group in CA (Figure 2F). After the chemical process of deacetylation, the carbonyl peak no longer appears, demonstrating successful removal of the acetal group and further the peak at the OH group near the 3200 cm^{-1} wavelength pronounces, which confirms the regeneration of cellulose[38] (Figure 2G). Figure 2I,J shows the fiber mat's water contact angle (WCA) measurements before and after deacetylation. The average WCA of electrospun SSA-CA fibers is 129.08 ± 0.46 ° and 108.69 ± 5.03 ° before and after deacetylation, respectively. A slight increase in hydrophilicity of the fiber mat was observed, again pointing to the successful transition from CA to regenerated cellulose. However, when observing WCAs over time, fiber mats after deacetylation demonstrate higher wettability with the water droplet showing lower WCAs of 46.57 ± 14.52 ° within 15 s (Figure S2A–C, Supporting Information). With natural cellulose being more hydrophilic than CA, it is expected to see lower WCAs, demonstrating deacetylation as a helpful procedure in converting CA fibers to regenerated cellulose fibers. Although surface treating fiber mats through plasma cleaning can alter their hydrophilic properties, deacetylated fiber mats provide a 198.51% higher vertical wicking rate (2 mm h^{-1}) than plasma cleaned fiber mats (0.67 mm h^{-1}) (Figure S2D-F, Supporting Information). The pore size of the stretchable paper was measured at 9.43 ± 4.16 μm (n = 100) with an average fiber mat thickness of 92.61 ± 10.17 μm (n = 25) at a fiber deposition time of 30 min.

As mentioned previously, commercially available paper such as Whatman brand paper has been widely used due to their wicking properties gaining the advantage over other paper substrates.[39] Whatman chromatography paper, with its moderate liquid flow and retention rate, can be attributed to its 180 μm thickness and 11 μm pore size. In contrast, the Whatman filter paper demonstrates greater liquid flow and retention rates due to its 20–25 μm pore sizes. Another available paper utilized is nitrocellulose membranes with a pore size of 0.45 μm. When comparing the stretchable paper's pore size with the pore sizes of commercially available papers and their flow and retention properties, the porosity of the stretchable paper has similar sizes compared to chromatography paper. However, the flow and retention rates of the stretchable paper differ from the flow rate and retention rates of chromatography paper; this can be attributed to different surface tension and pore sizes in the fiber mat. Although Whatman filter paper has superior wicking properties over our stretchable paper, optimizing the nanofibers allows for tunability in fiber morphology which may affect substrate flow rate and retention according to substrate requirements for bioelectronic applications. Therefore, porosity and fiber mat thickness can be tuned through electrospinning flow rate parameters and processing time. Additionally, fiber alignment can aid in the flow rate of liquids into the fiber mat, as fiber alignment can affect wicking properties.

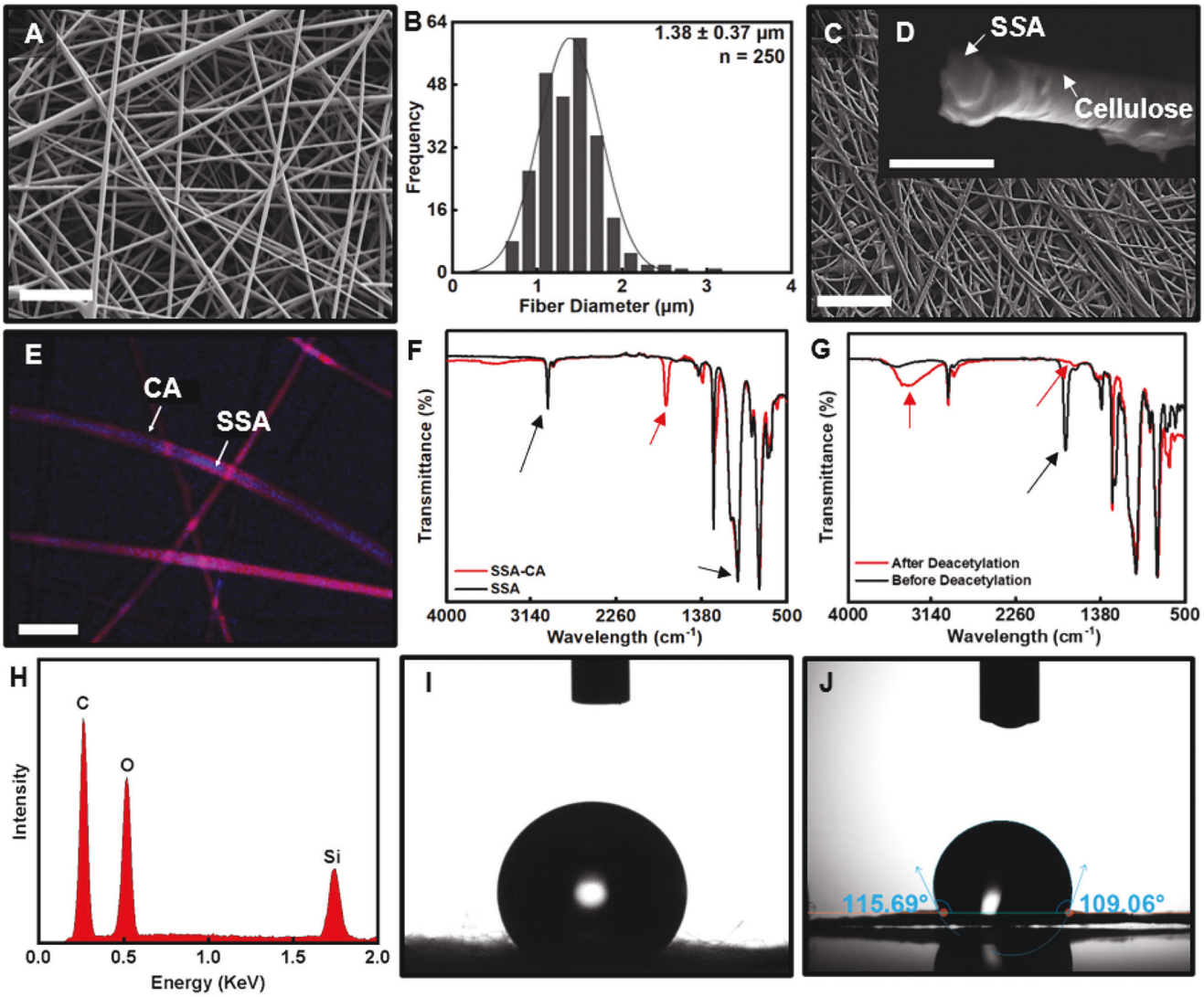

Figure 2. Surface characteristics of fibermat. A) SEM image of coaxial SSA-CA fibers (scale bar, 20 µm). B) Assessment of SSA-CA fiber diameter with an average fiber diameter of 1.38 ± 0.37 µm (n = 250). C) SEM image of coaxial SSA-Cellulose fibers after deacetylation (scale bar, 20 µm). D) SEM cross-sectional image of a coaxial SSA-Cellulose fiber after deacetylation and freeze fracture exposing the core material with an average core diameter of 476.48 ± 60.77 nm (n = 50) and average sheath thickness of 267.01 ± 84.86 nm (n = 50) (scale bar, 1 µm). E) confocal microscopy of a coaxial SSA-CA fiber with fluorescent dyes of Rhodamine B for CA (Red) and Quinine for SSA (blue) (scale bar, 5 µm). F) FTIR spectrum of SSA elastomer (black) and coaxial SSA-CA fiber mat (red). The spectrum indicates a presence of both silicone and cellulose acetate demonstrated at 1019 cm^{-1} and 1738 cm^{-1} for the siloxane group and the carbonyl group, respectively. G) FTIR spectrum of SSA-CA fiber before (black) and after (red) deacetylation. The sheath CA become cellulose after deacetylation demonstrated by the reduction in transmittance at the 1738 cm^{-1}. H) EDS analysis of coaxial SSA-CA fibers showing peaks of carbon and oxygen from CA and a silicone peak from the SSA. WCAs of fiber mats I) before and J) after deacetylation exhibiting 129.08 ± 0.46 ° and 108.69 ± 5.03 °, respectively.

Energy Dispersive X-ray Spectroscopy (EDS) analysis displayed the elemental composition of the SSA-CA fiber mat. The EDS spectrum shows a more significant peak from carbon, a lesser peak in oxygen, and an even lesser peak in silicone. In contrast, pure CA membranes have pronounced carbon and oxygen peaks[40] and SSA has a higher peak in silicone (Figure 2H). The surface elemental composition of SSA-CA coaxial fibers indicates that both CA and SSA are present (Figure S3A,B, Supporting Information) with minimal blending during electrospinning. More surface analyses of the fiber mat were analyzed using an optical profilometer to investigate the surface roughness before and after deacetylation (Figure S3C,D, Supporting Information). The fiber mat before deacetylation had a roughness average value of 10.16 µm, whereas the fiber mat showed a roughness average value of 5.33 µm after deacetylation. The reduction in surface roughness of the fiber mat after deacetylation can also indicate the increase in hydrophilicity of the deacetylated fiber mats over fiber before deacetylation. When comparing the fiber mat after deacetylation to commercially available Whatman filter paper, the surface roughness of the deacetylated fiber mats is lower than that of Whatman paper (12.2 – 13.9 µm) and similar to multipurpose printer paper (5.3 µm);[41] and shows that the

fiber mat after deacetylation falls within the range of other paper's average roughness measured in literature.[42] Furthermore, with the SSA-CA fiber mat made of cellulose and silicone materials, the biocompatibility was tested by laminating the fiber mat (20 mm × 30 mm) on skin for three days (Figure S3E,F, Supporting Information). After three days of lamination of the fiber mat to the skin, the fiber mat showed no visible sign of skin irritation or redness.

2.3. Mechanical Characteristics of Stretchable Paper

As previously mentioned, device performance for skin wearable devices is reliant on the efficacy in conformal contact with skin. Investigating the mechanical properties of the fiber mat to surpass the stretchability of paper-based substrates is an important criterion; however, ensuring this stretchability is suitable for electronics is equally important to ensure adequate device performance. **Figure 3**A,B demonstrates the biomechanics properties of a CA fiber mat compared to the SSA-CA fiber mat. The CA fiber mat without the silicone core exhibits a high tensile strength (3.20 ± 1.51 MPa) and high modulus of elasticity (130.97 ± 2.92 MPa) with a low percent strain at max tensile strength (18.60 ± 1.83%); however, the SSA-CA fiber mat shows a 13.13% decrease in tensile strength (2.78 ± 0.56 MPa) and low modulus of elasticity (32.02 ± 9.35 MPa) with a 139.41% increase in percent strain at max tensile strength (44.53 ± 6.34%) (Figure 3A). The linear region of the curve in Figure 3A, outlined by the green dotted box, shows where both CA and SSA-CA fiber mats start to show signs of plastic deformation. The CA fiber without the silicone core only shows a percent strain before deformation occurs at 0.80 ± 0.53%. In contrast, the SSA-CA fiber mat shows a percent strain of 2.27 ± 0.70% before deformation occurs, a 183.75% increase from the fiber mat without the silicone core (Figure 3B). Commercially available Whatman paper and other cellulose-based papers also exhibit low percent strains of 1–2%[43,44] before plastic deformation occurs, with maximum percent strains of less than 10% before breakage occurs.[45] Compared to Whatman grade cellulose papers, the fabricated SSA-CA fiber mat shows more percent strain before plastic deformation and breakage occur.

We can also verify that the integrity of the silicone core remains unchanged after deacetylation occurs. The SSA-cellulose II coaxial fibrous mat showed an elastic modulus of 8.64 ± 3.07 MPa and a 2.47 ± 0.23% percent strain before deformation occurs. It is expected to see higher elastic moduli from cellulose-based materials than cellulose acetate substrates which is why the SSA-Cellulose II fiber yields a higher elastic modulus. However, the percent strain before plastic deformation demonstrates a smaller standard deviation in percent strain, which confirms insignificant stretchable property changes after the deacetylation.

To further increase the hydrophilicity of the SSA-CA fiber mat after deacetylation for paper-based bioelectronics applications, we explored plasma treating the SSA-CA fiber mats and treating them with glycidoxypropyldimethoxymethylsilane (3G). The effect of chemical treatment on the biomechanics was tested. Figure 3C shows the biomechanics of each chemical process; the plasma-treated paper (red) displays the highest tensile strength, yet it is the chemical process with the lowest yield percent strain. The 3G-treated paper (blue) has the lowest tensile strength (0.16 ± 0.06 MPa) with a moderate yield percent strain (2.0 ± 1.93%). Although chemical treatment is advantageous to ensure a hydrophilic surface, there are slight tradeoffs in percent strain before deformation occurs. The 3G-treated paper offers the best hydrophilic surface but the lowest mechanical properties. The optimal chemical treatment for the hydrophilicity of the fiber mat's surface lies between the deacetylated fiber mat and the plasma cleaned fiber mat after deacetylation. To further quantify permeability, three different fiber mats (3G treated fiber mats, deacetylated fiber mats, Plasma treated fiber mats) and Whatman grade 410 filter paper were soaked in a Phosphate-buffered saline (PBS) solution (pH 7.4) for four hours at a temperature of 37 ^{0}C to observe water retention and swelling ratio (Figure S2I,J, Supporting Information). The swelling ratio for the 3G treated fiber mat, deacetylated fiber mat, plasma treated fiber mat, and Whatman filter paper was calculated at 8.22%, 17.56%, 25.60%, and 30.81% respectively. With Whatman paper having superior wicking and hydrophilic properties, the plasma treated SSA-Cellulose fiber mat yields a near similar swelling ratio to Whatman filter paper. Permeability of the SSA-Cellulose fiber mat with the presence of conductive paint spray coated onto the fiber mat was also assessed by using the fiber mat in an electrochemical setup to measure the oxidation reduction potential of water (Figure S2K, Supporting Information). The conductive SSA-Cellulose fiber mat, serving as the working electrode, was immersed in water along with an Ag/AgCl reference electrode showing the open circuit potential to be measured as −99.74 mV. Lastly, with the conductive SSA-Cellulose fiber mat submerged in PBS, the change in electrode impedance was measured over time with the electrode impedance measured at 835.30 Ω after twenty-five minutes (Figure S2L, Supporting Information).

The porous, stretchable, nonwoven fibrous electronic substrates offer many benefits for applications regarding skin interfaced devices. A 3D fibrous architecture of the substrate conformally laminated on the skin allows for better mass transfer of biofluids and airflow.[18,46] Additionally, with skin reaching percent strains of 30% with varying percent strain around areas of the body, having a stretchable yet robust fibrous structure with comparable mechanical properties to skin will aid in long-term device performance while providing compatibility, inhibiting issues with sweat accumulation and skin irritation. Figure 3D,E shows the SSA-CA fiber stretched state at 20% that the fibers bundle together and align their selves in the direction of the load, in contrast to fibers without the silicone core where micro tears are visible after strain (Figure S4, Supporting Information). The SSA-CA fiber structures are void of microcracks that could highlight the CA sheath taking advantage of the stretchability from the SSA core. The minimal polymer intermixing in the sheath and fibrous architectures aid in enhancing tolerance to mechanical distortion, especially stretching, without tear and surface crack on a single fiber.

Literature has shown other forms of stretchable paper in composite materials, such as works by Noguchi et al. and Wongvasana et al. These works discuss the fabrication of a cellulose/rubber composite nanofiber showing improved elongation at the break of the composite.[47,48] The authors mentioned tradeoffs between strength and ductility when polymers and elastomers are interfaced with each other. However, the tradeoff rule is unapplied to their material compared to their cellulose-rubber nanofiber

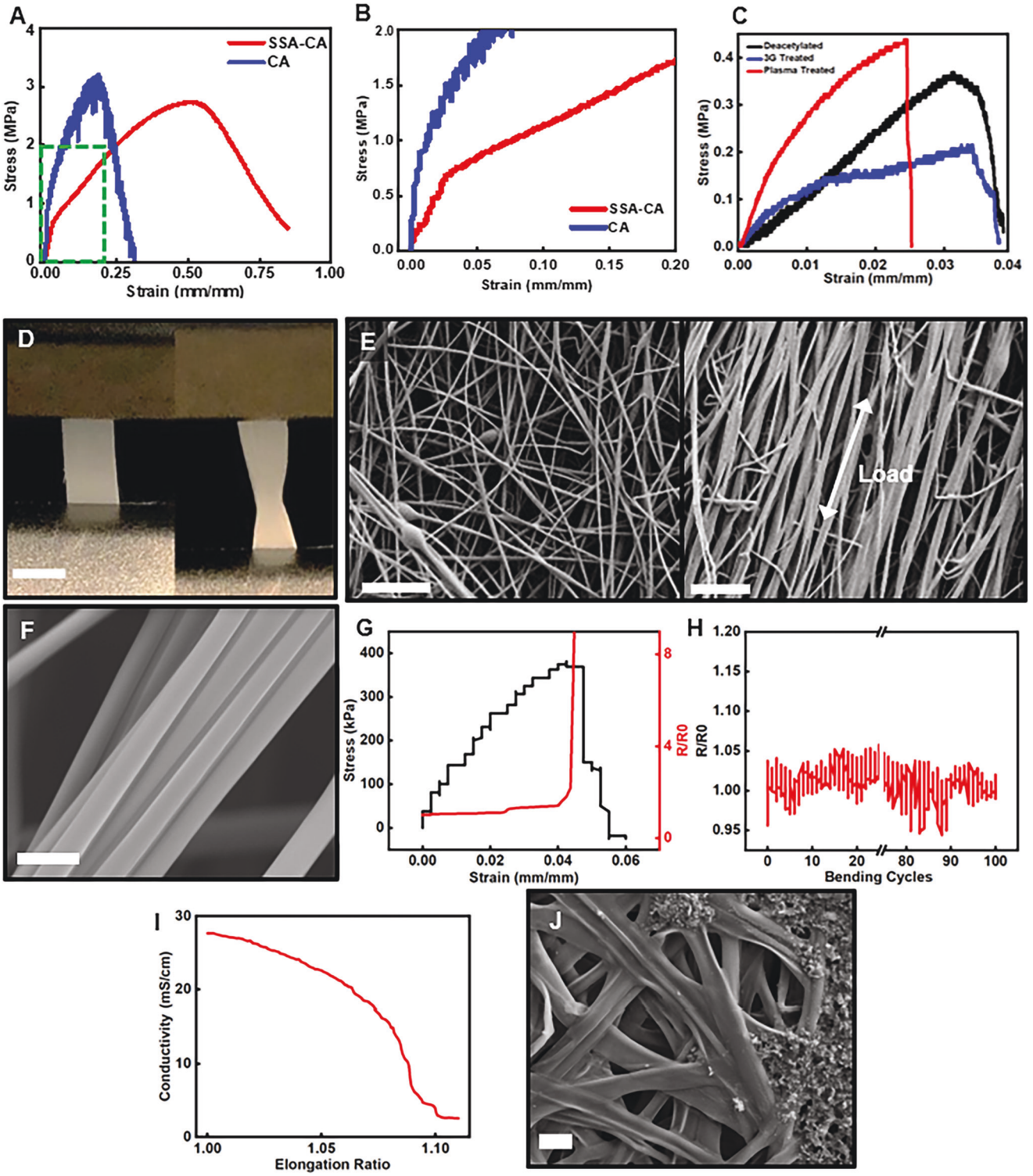

Figure 3. Mechanical properties of core-sheath structure. A) Stress-strain curve of SSA-CA fibers (red) compared to CA fibers (without elastomeric core) (blue). B) The enlarged graph of the green dotted box of (A) demonstrate an improvement of percent strain from the addition of the SSA core in plastic deformation region. C) Mechanical testing of a deacetylated fiber mat (black), a deacetylated fiber mat after 3-glycidyloxypropyl treated (blue), and a deacetylated fiber mat after plasma treatment (red). D) Image of SSA-CA fibers at no strain (left) and 20% strain (right) (scale bar, 5 mm). E) SEM images of SSA-CA fiber at 0% strain (left) and 20% strain (right) (Scale bar, 20 µm). F) SEM image of single bundle of fibers under 20% strain (Scale bar, 2 µm). G) Graph demonstrating change in resistance of a SSA-Cellulose fibermat coated with carbon paint while stretching. H) Graph showing change in resistance under bending cycles at a bending radius of 4 mm. I) Graph showing conductivity with change in length of fiber mat upon stretching. J) SEM Image of SSA-Cellulose fibermat with conductive paint showing area near fracture point with no visible microcracks after being stretched until break (Scale bar, 2 µm).

composite. Comparing this to our material, however, because our fiber material is a core-sheath structure of solid polymer and solid elastomer rather than a mixed polymer/elastomer composite, both core and sheath material retain their material characteristics which for the elastomeric core does not hinder the ductility, which can be seen with the mechanical properties of the core-sheath fiber with and without the CA sheath material. Although Noguchi et al. proposed that the cellulose nanofiber's hydrophilic nature efficiently mixes with the rubber material's hydrophobic properties, a core-sheath structure allows natural hydrophilic properties on the surface of the fiber.

Moreover, Zang et al. utilized graphene paper as a high-performance supercapacitor by applying it to an elastomeric film that was pre-strained 1.5 – 5 times its original dimension.[49] Upon loading the graphene paper, the film was released, creating a crumpled graphene paper over the stretchable film. Although the graphene paper and elastomer film create this layered material with mismatching properties, the paper having ridges and wrinkles from the release of the pre-strained film allows for stretching cycles to occur with minimal changes in capacitance. Creating these wrinkles in the graphene paper also allows for better flexibility under bending cycles.[50] The layered crumpled graphene paper material exhibits flexibility attributed to the wrinkles along the paper. However, its stretchability relies on the elastomeric film layer underneath the crumpled paper, while the core-sheath SSA-CA structure allows for only the cellulose material to be exposed. This core-sheath configuration of elastomer to paper sheath enables the formation of more complex patterning techniques for bioelectronic devices. Other stretchable paper-based devices, such as those that utilize origami folding techniques,[8] have also become advantageous for textiles and wearable electronics applications. However, with the 2D papers formed and folded into complex structures using origami techniques, flexibility, and conformability can be lost as the 3D architectures for complex electronics. The SSA-CA fiber mat's thin nature becomes advantageous for future wearable technology, in addition to stretchability, because of its ability to conform and become flexible to different shapes and curvatures.

The biomechanics of the SSA-Cellulose fiber mat with conductive paint and the resistivity during stretching was analyzed. Fiber mats were plasma cleaned for one minute and spray coated with a 3:1 ratio of deionized water and electric paint. The copper tape was placed on the coated fiber mat to measure the change in resistance as the strain was applied across the fiber mat. Figure 3G demonstrates the spray coated SSA-cellulose fiber mat undergoing strain with the change in resistance displayed. After the deionized water permeated through the fiber mat, the carbon particles from the electric paint remained toward the surface of the fiber mat post drying. With a paint layer of 459.98 ± 60.19 nm over the fiber mat, the spray coated electric paint has negligible effects on the biomechanics of the fiber mat with a thin coating layer over the fibers (Figure S2G, Supporting Information). The resistivity during increased strain remains unchanged until after plastic deformation, with a percent change in increased resistance of 41%, which occurs at a percent strain of 4%. Figure 3H shows the spray coated fiber mat undergoing bending cycles (n = 100) while measuring change in resistance with a 5.66% increase in change of resistance. As mentioned earlier, most ridged devices fail at a strain of 3%. With inexpensive fabrication steps and materials, the designed fiber mat yields a slight increase in percent strain with adequate change in resistance. Figure 3I shows conductivity of the spray coated fiber mat along with elongation. The measured conductivity shows a decrease from 27.67 to 2.57 mS cm^{-1}, which shows low electrical conductivity compared to other flowable electrodes with higher electrical conductivity; however, Figure 3J SEM image shows no visible signs of microcracks of neighboring fibers upon break.

2.4. Stretchable Paper in Applications for Papertronics

The fabricated stretchable papers can serve as a substrate for biointegrated bioelectronics, as demonstrated on regular filter papers and elastomeric polymer films. The 3D fibrous structured stretchable nonwoven cellulose mat adapts manufacturing approaches, including ink and wax printing, bioactive molecule inoculation, and patterns with laser cutters.[51] To test a wide range of engineering processability, we constructed a microbial fuel cell (MFC) device that requires various processing techniques and is representative of papertronic devices for bio-energy and biosensing applications.[52,53] Before fabricating the individual electrodes, the paper sheets were plasma treated for one minute and then treated with 3G to loosen the paper fiber and increase the hydrophilicity of the paper. The MFC was fabricated by stacking the anode, membrane, and cathode in a sandwich structure (**Figure 4**A,B). The anode was engineered by immersing the paper in the mixture of conductive polymer PEDOT: PSS and dimethyl sulfoxide (DMSO) for 5 h and dried overnight at room temperature. Then, *Shewanella oneidensis*, an electrogenic bacteria demonstrating high metabolic rate and power generation, was inoculated into the 3D fibrous structure (Figure 4C).[54] Wax penetration formed the proton exchange membrane (PEM) so that the metabolically produced protons can be diffused to the cathode while the electrons move externally along the circuit (Figure 4D). Due to the cathode material having a low over-potential, the cathode was prepared by introducing an Ag_2O catalyst diluted in the PEDOT: PSS solution (Figure 4E). Finally, the copper tape was connected to the anode and cathode to analyze electronic characteristics. The power outputs and polarization curves were acquired from the stretchable paper-based MFCs by measuring the voltage values at various external resistors and calculating the corresponding electrical current density values (Figure 4F). The MFC could generate up to ≈11 μW cm^{-2}, within the range of paper MFC standard performance. The stretchable paper-based MFC device has comparable power outputs to stackable MFC devices in the field. The SSA-Cellulose fibermats demonstrate retention of paper-like characteristics such as: biocompatibility and non-toxicity for creating an environment for inoculation of the *Shewanella oneidensis* bacteria and hydrophilicity for the bacteria to have proper fixation onto the fibers. Indeed, the stretchable MFC highlights that the SSA-cellulose capable of adapting conventional fabrication processes and universal approaches for creating papertronics.

With the work presented with the microbial fuel cell, other works have utilized cellulose with other materials to generate electricity or act as a conductive electrode. Ando et al. developed a nanofiber stimulation electrode using chitosan nanofibers. With their average fiber diameters ranging from 20–50 nm, the

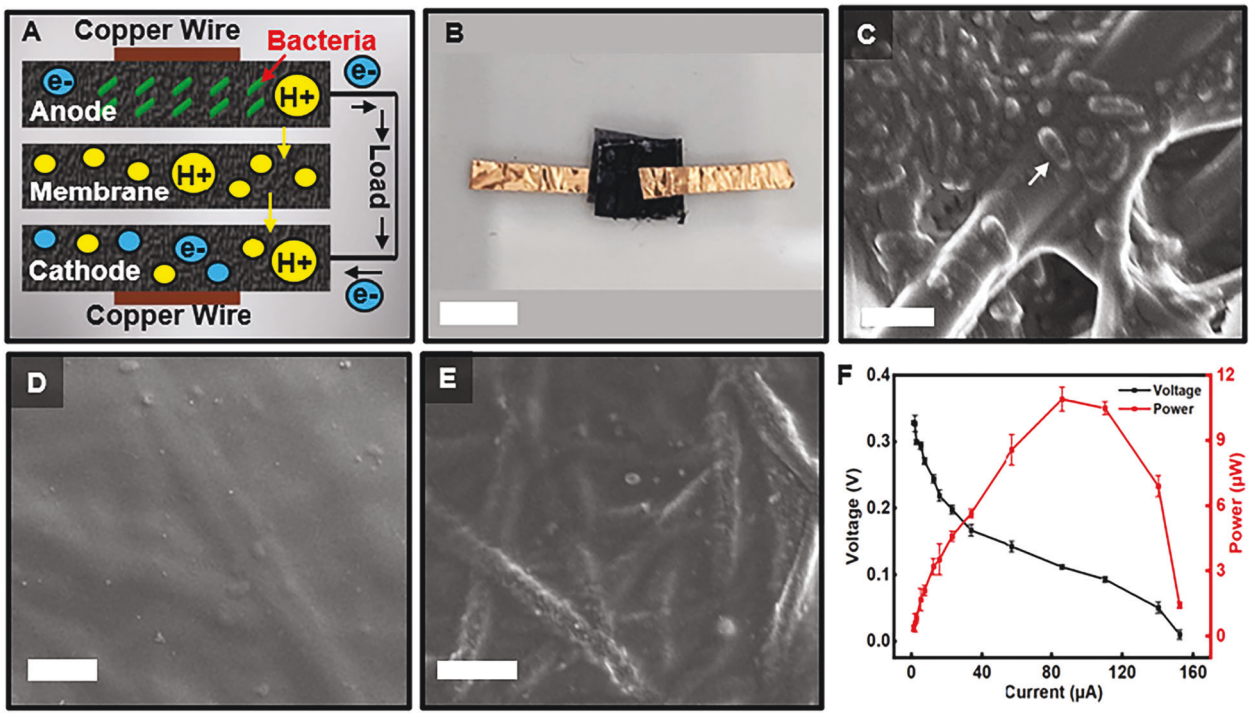

Figure 4. MFC Device using stretchable paper. A) Schematic and mechanism of paper-based MFC device. B) Image of MFC device assembly (scale bar, 2 mm). C) SEM image of *Shewanella oneidensis* bacteria (white arrow) and anode material over fibers (scale bar, 2 μm). D) SEM image of wax membrane material over fibers (Scale bar, 5 μm). E) SEM image of cathode material over fibers (Scale bar, 4 μm). F) Power outputs and polarization curves of the fabricated MFC on the stretchable paper demonstrating a max power output of 10.5 μW.

maximum strain measured until breakage was 6.1 ± 1.8, which they mention is greater than most cellulose-based nanofiber substrates.[55] With our stretchable paper, the maximum strain before breakage occurs is 45% at a fiber diameter of 700 to 1200 nm. Additionally, the stretchable paper, in its deacetylated state, has a maximum strain of 4–6% before breakage occurs, comparable to the chitosan nanofibers' mechanical properties. The SSA-CA fiber mat's advantage over their chitosan nanofibers is the larger fiber diameters, which create larger pore sizes that correlate to the permeability and breathability of the worn device. Furthermore, when it comes to the change in resistance of the stretchable paper compared to the chitosan nanofibers, both show a similar change in resistance at 4–6% before breakage occurs despite the stretchable paper being fully coated with conductive paint while chitosan nanofibers being patterned with carbon nanotubes.

Electrospinning, a favorable technique for creating nanofibers, is widely adopted due to its controllability in production of fibers and low cost in fabrication.[56] Pairing the cost-effective fabrication technique with abundance of cellulose materials only furthers the impact of creating inexpensive devices with affordable materials with controlled stretchability. The ability to utilize electrospinning to create stretchable fibers can have advantages in creating fiber mats of different dimensions and various fiber morphologies depending on the requirements of the material. With preparation times of cellulose and silicone solutions being made within hours for electrospinning, the complexity in the fabrication of an SSA-CA fiber mat becomes simple with the benefit of creating several amounts of fiber mats on demand, making these parameters and system setup up repeatable enough for scalable manufacturing purposes for a variety of bioelectronic devices and pharmaceutical materials.[57] When comparing the tunability of stretchable paper via electrospinning to commercially available papers such as Whatman paper, the applications of stretchable paper can become advantageous for skin-interfaced bioelectronics devices and conventional paper-based bioelectronics. In contrast, Whatman grade papers are limited to skin-based applications due to the inability to match the mechanical properties of the skin.

3. Conclusion

In summary, we engineered a paper-based substrate with elastic properties through coaxial nanofibers of a silicone elastomer core and a cellulose-based polymer sheath. The individual fibers were tuned the mechanical properties to become stretchable while retaining the chemical and physical characteristics of paper. This approach of fabricating a stretchable paper demonstrates a flexible substrate for soft bioelectronics applications, mimicking the mechanical structure of the epidermis while retaining the essential characteristics of cellulose-based materials to create inexpensive electronics. The silicone elastomer-cellulose coaxial nanofibrous mats were demonstrated in an assembly build of an MFC device and as a stretchable paper fluidic device. Both applications highlight the usability of this fiber mat for stretchable and flexible bioelectronics and paper-based electronics. The SSA-CA fiber mat was fabricated through systematic studies to provide substantial evidence of a core-sheath structure of silicone and

cellulose; however, limitations in substrate permeability posed an issue when converting CA into cellulose II during the deacetylation process; soaking the fiber mat over 24 h in the sodium hydroxide solution hinders the ease of thoroughly removing the polymer from the pores.

Preliminary testing already shows the deacetylated fiber mat to be capable of retaining wax patterns from crayons to create a paperfluidic device, allowing fluid to flow within the designed patterns (Figure S2H, Supporting Information); however, future work will explore other methods of deacetylation to loosen fibers and increase permeability through probe tip sonication during deacetylation. Additionally, electrospinning randomly aligned fibers will be compared to aligned fibers to investigate the effects of surface topography in relation to wettability along with mechanical property changes. Moreover, a primary focus will be to integrate inexpensive conductive electronics on this nanofibrous substrate for biochemical on-skin sensing applications to further emphasize the capabilities and applications of this paper-based stretchable substrate. The stretchable paper holds significant potential, capable of bridging the gap between papertronics and soft bioelectronics, to be realized as an advantageous alternative to standard substrates for biointegrated bioelectronics.

4. Experimental Section

Materials: Cellulose Acetate Powder (30 000 MW), Dimethyl sulfoxide (DMSO), Dimethylformamide (DMF), Rhodamine B, Quinine Hemisulfate Salt Monohydrate, and Glycidoxypropyldimethoxymethylsilane were purchased from Sigma Aldrich (Milwaukee, WI). Sylgard 184 silicone elastomer kit (PDMS) was purchased from Ellsworth Adhesives (Germantown, WI). Liveo 7–9700 Soft Silicone Adhesive (SSA) Kit A and B were gifted from DuPont (Midland, MI). Sodium Hydroxide Pellets, Acetone, Trifluoracetic acid (TFA), Dimethylacetamide (DMA), and Ethanol were purchased from VWR (Radnor, PA). Tetrahydrofuran (THF) was purchased from Alfa Aesar (Ward Hill, MA). Circuit Drawing Kit with Conductive Ink by Circuit Scribe was purchased from Amazon (Conklin, NY). Electric Paint was purchased from Bare Conductive and applied with the Master Airbrush G233 Pro. PEDOT: PSS (Clevios PH1000) was purchased from Heraeus. The Shewanella species (MR-1) was acquired from the American Type Culture Collection (ATCC).

Coaxial Electrospinning: Coaxial SSA-CA nanofibers were fabricated through the MSK-NFES-3 benchtop electrospinning unit (Figure S1A, Supporting Information). The CA solution and SSA solution were placed into syringes (15.65 mL) and loaded into the electrospinning unit's automatic pump. 1.6 mm polypropylene female luer lock fittings were attached to the syringes, and Polytetrafluoroethylene (PTFE) tubing (2 mm ID × 4 mm OD) was joined to the luer lock on one side, with the other placed into a push to connect pneumatic straight fitting joint (M6 – 4 mm ID). To ensure encapsulation of the SSA elastomer via the CA polymer, the needles chosen for the core and sheath solution were 21 gauge and 15 gauge, respectively. The flow rate for the CA solution was set to 1.0 mL h^{-1} and the SSA solution to 0.2 mL h^{-1}. The coaxial electrospinning system was designed vertically with a tip-to-collector distance of 12 cm and a voltage of 9.2 kV to form the desired Taylor cone (Figure S1B, Supporting Information). The collector plate was placed underneath the coaxial needle for collection of the randomly aligned fibers; however, use of a rotating mandrel can also be integrated into the electrospinning unit for controlled fiber alignment. The stationary collector plate was fitted with aluminum foil to collect the deposited fibers at room temperature (≈21.3 °C) at a processing time of 30 min. Dupont's SSA has a pot life of 130 min after mixing both parts. The fiber mats were placed in an oven for 24 h at 100 °C to expedite the curing process after fiber deposition. Systematic studies of a suitable solvent system for CA were carried out in weight percent between 15 and 23 using three solvents: TFA, a 2:1 ratio of Acetone to DMA, and an 85:15 ratio of acetone to DMF (Table S1, Supporting Information).

Similarly, the optimization of an elastomeric core solution for coaxial electrospinning was explored using Dow's Sylgard 184 silicone elastomer kit forming PDMS and DuPont's Liveo 7–9700 SSA kit. PDMS was used in a base-to-curing ratio of 30:1 and 10:1 with an added 10% of THF to reduce solution viscosity. The varying core solutions were investigated with the three solvent systems at varying weight percent of the sheath solution. DuPont's SSA kit utilizes a 1:1 ratio of a two-part silicone system; the SSA solution was studied with this ratio at different percentages of added THF (0%, 10%, 20%) to monitor the effects of solution viscosity during coaxial electrospinning (Table S3, Supporting Information).

Deacetylation of Nanofibers: Post curing, the fiber mats were cut into squares and framed into a window using polyimide (PI) tape on both sides of the fiber mat. The fiber mats were soaked in a 0.05 M solution of sodium hydroxide and ethanol (NaOH/EtOH) and were water bath sonicated for 45 min at 60 °C. Then, the fiber mats we left in the solution for 24 h at 60 °C. The fiber mat was removed from the NaOH/EtOH solution, thoroughly rinsed with deionized water, and dried at room temperature overnight.

Characterization: Zeiss observed the SSA-CA fiber morphology using the Supra 55 VP field emission scanning electron microscopy. Fiber diameter was analyzed by measuring 250 measurements and porosity size was analyzed with 100 measurements through ImageJ. The fiber cross-section was done through freeze fracture by soaking the SSA-CA fiber mat in a liquid nitrogen chamber for ten days, then splitting the fiber mat in half, exposing the core encapsulated by the sheath. Confocal microscopy was used as a secondary method to visualize the core-sheath structure of the fiber through Zeiss's 2-photon LSM 880 confocal microscope. Fluorescent dyes added to the CA polymer solution and the SSA elastomer aided in visualizing the core-sheath structure of the SSA-CA fiber, noted by the blue dye for the core and the red dye for the sheath of the CA sheath (Figure 2E). The Alpha II FTIR Spectrometer analyzed the chemical structure of SSA-CA by Bruker Optics Inc. Elemental peaks were observed using the Supra 55 VP energy dispersive spectroscope (EDS). The Veeco NT1100 Optical Surface Profiler measured the surface roughness of the fiber mats before and after deacetylation. Contact angle measurements were done on the Theta Lite Optical Tensiometer by Biolin Scientific with angles measured on a 4 µL drop of deionized water. Mechanical testing of 10 mm × 5 mm SSA-CA fiber mats ($n = 3$) was performed on the ESM303 Mark 10 System using a 25 N force gauge at a 0.5 mm min^{-1} strain rate. Electronic performance tests were performed with a digital multimeter (Keysight, 34460A) to record the real-time resistance.

Supporting Information

Supporting Information is available from the Wiley Online Library or from the author.

Acknowledgements

The authors thank the staff of the Health Sciences Core Facility (HSCF) and Analytical and Diagnostics Laboratory (ADL) at Binghamton University for technical support. Funding: This work was supported by the National Science Foundation (ECCS # 2020486 and #1920979, NSF CAREER CBET # 2238173). The authors acknowledge the support of the Small-Scale Systems Integration and Packaging Center of Excellence (S3IP).

Conflict of Interest

The authors declare no conflict of interest.

Author Contributions

J.S.D., M.S.B., and A.K. led the development idea and designed the experiments. J.D. performed the experiments and wrote the paper. Z.R. and

A.E. provided the electrogenic bacteria, fabricated the stackable MFC device, produced the polarization curves for power output, and contributed to writing the corresponding section. S.C. oversaw the development for creating stackable MFCs. A.K. supervised this work, provided guidance, and assisted in drafting the manuscript as the corresponding author.

Data Availability Statement

The data that support the findings of this study are available in the supplementary material of this article.

Keywords

coaxial electrospun cellulose fibers, paper-based electronics, soft bioelectronics, stretchable fibrous electronic substrates

Received: June 12, 2023
Revised: September 14, 2023
Published online:

[1] Y. Lin, D. Gritsenko, Q. Liu, X. Lu, J. Xu, *ACS Appl. Mater. Interfaces* **2016**, *8*, 8345.
[2] S. K. Mahadeva, K. Walus, B. Stoeber, *ACS Appl. Mater. Interfaces* **2015**, *7*, 8345.
[3] N. Wada, T. Fujie, R. Sasaki, T. Matsushima, K. Takahashi, *Polym J* **2022**, *54*, 735.
[4] L. Gao, C. Zhu, L. Li, C. Zhang, J. Liu, H.-D. Yu, W. Huang, *ACS Appl. Mater. Interfaces* **2019**, *11*, 25034.
[5] Y. Zhang, C. Zhang, Y. Wang, *Nanoscale Adv* **2021**, *3*, 6040.
[6] T.-T. Tsai, T.-H. Huang, C.-J. Chang, N. Y.-J. Ho, Y.-T. Tseng, C.-F. Chen, *Sci. Rep.* **2017**, *7*, 3155.
[7] E. Bihar, S. Wustoni, A. M. Pappa, K. N. Salama, D. Baran, S. Inal, *npj Flexible Electron.* **2018**, *2*, 30.
[8] X. Chen, Y. Li, X. Wang, H. Yu, *ACS Appl. Mater. Interfaces* **2022**, *14*, 36227.
[9] C. Wang, R. Wu, H. Ling, Z. Zhao, W. Han, X. Shi, G. F. Payne, X. Wang, *npj Flexible Electron.* **2022**, *6*, 12.
[10] Z. Dong, H. Liu, X. Yang, J. Fan, H. Bi, C. Wang, Y. Zhang, C. Luo, X. Chen, X. Wu, *npj Flexible Electron.* **2021**, *5*, 6.
[11] A. Russo, B. Y. Ahn, J. J. Adams, E. B. Duoss, J. T. Bernhard, J. A. Lewis, *Adv. Mater.* **2011**, *23*, 3426.
[12] N. Hussain, M. Mehdi, S. H. Siyal, R. K. Wassan, S. Hashemikia, M. N. Sarwar, T. Yamaguchi, I. S. Kim, *J. Appl. Polym. Sci.* **2021**, *138*, 51381.
[13] M. D. Dickey, in *Stretchable Bioelectronics for Medical Devices and Systems*, Springer International Publishing, Cham, New York **2016**, pp. 3–30.
[14] W. Zhang, Z. Jing, Y. Shan, X. Ge, X. Mu, Y. Jiang, H. Li, P. Wu, *J Mater Chem A Mater* **2016**, *4*, 17483.
[15] A. K. Yetisen, J. L. Martinez-Hurtado, B. Ünal, A. Khademhosseini, H. Butt, *Adv. Mater.* **2018**, *30*, 1706910.
[16] F. Molina-Lopez, T. Z. Gao, U. Kraft, C. Zhu, T. Öhlund, R. Pfattner, V. R. Feig, Y. Kim, S. Wang, Y. Yun, Z. Bao, *Nat. Commun.* **2019**, *10*, 2676.
[17] Y. Wang, T. Yokota, T. Someya, *NPG Asia Mater* **2021**, *13*, 22.
[18] M. S. Brown, M. Mendoza, P. Chavoshnejad, M. J. Razavi, G. J. Mahler, A. Koh, *Adv. Mater. Technol.* **2020**, *5*, 2000242.
[19] D. Han, A. J. Steckl, *ChemPlusChem* **2019**, *84*, 1453.
[20] J. Xue, T. Wu, Y. Dai, Y. Xia, *Chem. Rev.* **2019**, *119*, 5298.
[21] M. Li, Y. Zheng, B. Xin, Y. Xu, *Ind. Eng. Chem. Res.* **2020**, *59*, 6301.
[22] S. Vats, M. Anyfantakis, L. W. Honaker, F. Basoli, J. P. F. Lagerwall, *Langmuir* **2021**, *37*, 13265.
[23] H. Zhou, Z. Shi, X. Wan, H. Fang, D.-G. Yu, X. Chen, P. Liu, *Nanomaterials* **2019**, *9*, 843.
[24] A. Kramar, F. J. González-Benito, *Polymers (Basel)* **2022**, *14*, 286.
[25] N. Tulos, D. Harbottle, A. Hebden, P. Goswami, R. S. Blackburn, *ACS Omega* **2019**, *4*, 4936.
[26] G. Siqueira, J. Bras, A. Dufresne, *Polymers (Basel)* **2010**, *2*, 728.
[27] S. E. López, J. Salazar, *J Fluor Chem* **2013**, *156*, 73.
[28] J. N. Lee, C. Park, G. M. Whitesides, *Anal. Chem.* **2003**, *75*, 6544.
[29] A. Xu, L. Chen, Y. Wang, R. Liu, W. Niu, *Polymers (Basel)* **2019**, *11*, 845.
[30] M. W. Frey, *Polymer Reviews* **2008**, *48*, 378.
[31] C.-W. Kim, D.-S. Kim, S.-Y. Kang, M. Marquez, Y. L. Joo, *Polymer (Guildf)* **2006**, *47*, 5097.
[32] N. Basma, P. L. Cullen, A. J. Clancy, M. S. P. Shaffer, N. T. Skipper, T. F. Headen, C. A. Howard, *Mol. Phys.* **2019**, *117*, 3353.
[33] J. Muzart, *Tetrahedron* **2009**, *65*, 8313.
[34] K. Izdihar, H. R. Abdul Razak, N. Supion, M. K. A. Karim, N. H. Osman, M. Norkhairunnisa, *Appl. Sci.* **2021**, *11*, 1172.
[35] J. H. Cho, Y. Gao, J. Ryu, S. Choi, *ACS Omega* **2020**, *5*, 13940.
[36] J. H. Cho, Y. Gao, S. Choi, *Sensors* **2019**, *19*, 5452.
[37] R. Wei, Y. He, J. Liu, Y. He, W. Mi, R. Yuen, J. Wang, *Materials* **2017**, *10*, 316.
[38] F. Ahmed, A. Ayoub Arbab, A. W. Jatoi, M. Khatri, N. Memon, Z. Khatri, I. S. Kim, *Ultrason. Sonochem.* **2017**, *36*, 319.
[39] A. Singh, D. Lantigua, A. Meka, S. Taing, M. Pandher, G. Camci-Unal, *Sensors* **2018**, *18*, 2838.
[40] A. M. Pandele, F. E. Comanici, C. A. Carp, F. Miculescu, S. I. Voicu, V. K. Thakur, B. C. Serban, *Vacuum* **2017**, *146*, 599.
[41] A. T. Vicente, A. Araújo, D. Gaspar, L. Santos, A. C. Marques, M. J. Mendes, L. Pereira, E. Fortunato, R. Martins, *Nanostruct. Sol. Cells* **2017**,*1*, 35.
[42] A. Alam, A. Manuilskiy, J. Thim, M. O'nils, J. Lindgren, J. Lidén, *Nord Pulp Paper Res J* **2012**, *27*, 662.
[43] I. Levy, A. Nussinovitch, E. Shpigel, O. Shoseyov, *Cellulose* **2002**, *9*, 91.
[44] S. M. Khan, J. M. Nassar, M. M. Hussain, *ACS Appl. Electron. Mater.* **2021**, *3*, 30.
[45] M. Cocca, L. D'arienzo, L. D'orazio, *ISRN Mater. Sci.* **2011**, *2011*, 863083.
[46] M. M. Leena, K. S. Yoha, J. A. Moses, C. Anandharamakrishnan, in *Innovative Food Processing Technologies*, Elsevier, New York **2021**, pp. 634–650.
[47] B. Wongvasana, B. Thongnuanchan, A. Masa, H. Saito, T. Sakai, N. Lopattananon, *Polymers (Basel)* **2023**, *15*, 1274.
[48] T. Noguchi, M. Endo, K. Niihara, H. Jinnai, A. Isogai, *Compos. Sci. Technol.* **2020**, *188*, 108005.
[49] J. Zang, C. Cao, Y. Feng, J. Liu, X. Zhao, *Sci. Rep.* **2014**, *4*, 6492.
[50] D. A. Dikin, S. Stankovich, E. J. Zimney, R. D. Piner, G. H. B. Dommett, G. Evmenenko, S. T. Nguyen, R. S. Ruoff, *Nature* **2007**, *448*, 457.
[51] M. Landers, A. Elhadad, M. Rezaie, S. Choi, *ACS Appl. Mater. Interfaces* **2022**, *14*, 45658.
[52] L. Liu, M. Mohammadifar, A. Elhadad, M. Tahernia, Y. Zhang, W. Zhao, S. Choi, *Adv. Energy Mater.* **2021**, *11*, 2100713.
[53] Z. Rafiee, M. Rezaie, S. Choi, *Biosens. Bioelectron.* **2022**, *216*, 114604.
[54] A. Elhadad, S. Choi, *Analyst* **2022**, *147*, 4082.
[55] D. Ando, T. F. Teshima, F. Zurita, H. Peng, K. Ogura, K. Kondo, L. Weiß, A. Hirano-Iwata, M. Becherer, J. Alexander, B. Wolfrum, *J Nanobiotechnology* **2022**, *20*, 491.
[56] S. Ramakrishna, K. Fujihara, W.-E. Teo, T. Yong, Z. Ma, R. Ramaseshan, *Mater. Today* **2006**, *9*, 40.
[57] S. Omer, L. Forgách, R. Zelkó, I. Sebe, *Pharmaceutics* **2021**, *13*, 286.